Remote Sensing of Environment 273 (2022) 112957

Contents lists available at ScienceDirect

Remote Sensing of Environment

journal homepage: www.elsevier.com/locate/rse

Response times of remote sensing measured sun-induced chlorophyll fluorescence, surface temperature and vegetation indices to evolving soil water limitation in a crop canopy

A. Damm [a,b,*], S. Cogliati [c], R. Colombo [c], L. Fritsche [a], A. Genangeli [d], L. Genesio [d], J. Hanus [e], A. Peressotti [f], P. Rademske [g], U. Rascher [g], D. Schuettemeyer [h], B. Siegmann [g], J. Sturm [a], F. Miglietta [d,i]

[a] Department of Geography, University of Zurich, Winterthurerstrasse 190, 8057 Zurich, Switzerland
[b] Eawag, Swiss Federal Institute of Aquatic Science and Technology, 8600 Dübendorf, Switzerland
[c] Remote Sensing of Environmental Dynamics Lab., DISAT, University of Milano-Bicocca, P.zza della Scienza 1, 20126 Milano, Italy
[d] Institute of Bioeconomy – IBE, National Research Council – CNR, Via Caproni 8, 50145 Florence, Italy
[e] Global Change Research Institute – CzechGlobe, Czech Academy of Sciences, Bělidla 986/4a, 60300 Brno, Czech Republic
[f] Department of Agricultural, Food, Environmental and Animal Sciences, University of Udine, Via delle Scienze 206, 33100 Udine, Italy
[g] Institute of Bio- and Geosciences, Plant Sciences (IBG-2), Forschungszentrum Jülich GmbH, 52428 Jülich, Germany
[h] European Space Agency, ESTEC, 2201, AZ, Noordwijk, the Netherlands
[i] Fondazione per il Clima e la Sostenibilità, Via Caproni, 8 50145 Florence, Italy

ARTICLE INFO

Jing M. Chen

Keywords:
Soil water limitation
Agricultural ecosystems
Multi-sensor remote sensing
Photochemical reflectance index
MERIS terrestrial chlorophyll index
Water band index

ABSTRACT

Vegetation responds at varying temporal scales to changing soil water availability. These process dynamics complicate assessments of plant-water relations but also offer various access points to advance understanding of vegetation responses to environmental change. Remote sensing (RS) provides large capacity to quantify sensitive and robust information of vegetation responses and underlying abiotic change driver across observational scales. Retrieved RS based vegetation parameters are often sensitive to various environmental and plant specific factors in addition to the targeted plant response. Further, individual plant responses to water limitation act at different temporal and spatial scales, while RS sampling schemes are often not optimized to assess these dynamics. The combination of these aspects complicates the interpretation of RS parameter when assessing plant-water relations. We consequently aim to advance insight on the sensitivity of physiological, biochemical and structural RS parameter for plant adaptation in response to emerging soil water limitation. We made a field experiment in maize in Tuscany (Central Italy), while irrigation was stopped in some areas of the drip-irrigated field. Within a period of two weeks, we measured the hydraulic and physiological state of maize plants in situ and complemented these detailed measurements with extensive airborne observations (e.g. sun-induced chlorophyll fluorescence (SIF), vegetation indices sensitive for photosynthesis, pigment and water content, land surface temperature). We observe a double response of far-red SIF with a short-term increase after manifestation of soil water limitation and a decrease afterwards. We identify different response times of RS parameter representing different plant adaptation mechanisms ranging from short term responses (e.g. stomatal conductance, photosynthesis) to medium term changes (e.g. pigment decomposition, changing leaf water content). Our study demonstrates complementarity of common and new RS parameter to mechanistically assess the complex cascade of functional, biochemical and structural plant responses to evolving soil water limitation.

1. Introduction

Anthropogenic caused global climate change continuously affects our ecosystems and releases a daily fingerprint in weather since 2012 (Sippel et al., 2020). Extreme events, i.e. heat waves, droughts, flooding, become more frequent and additionally impact ecosystem integrity and

* Corresponding author.
E-mail address: alexander.damm@geo.uzh.ch (A. Damm).

https://doi.org/10.1016/j.rse.2022.112957
Received 11 August 2021; Received in revised form 10 January 2022; Accepted 11 February 2022
Available online 28 February 2022

functioning in complex and manifold ways (Reichstein et al., 2013; Schuldt et al., 2020; Sippel et al., 2018; von Buttlar et al., 2018). Increasing evidence suggests that our capacity to unravel underlying interactions and feedbacks between climate dynamics, weather conditions and ecosystem functioning requires to go beyond pure climatological considerations and include impact perspectives in terms of alterations of carbon and water cycling (Reichstein et al., 2013; Smith, 2011). At the same time, sensitive concurrent observations of ecosystem functioning (e.g. carbon and water cycle dynamics) and abiotic environmental drivers for impactful events are pivotal to advance understanding but are still rare.

Remote sensing (RS) increasingly allows assessing valuable direct or indirect indicators of ecosystem functions and environmental driver across observational scales. Recent studies demonstrate suitability of RS to inform, for example, assessments of ecosystem carbon (Ciais et al., 2014; Ryu et al., 2019) and water exchange processes (Talsma et al., 2018; Wang and Dickinson, 2012). Besides the success of existing approaches under normal environmental conditions, biases were recently reported for RS based carbon exchange assessments under extreme climatic conditions (Miralles et al., 2019; Stocker et al., 2019). Furthermore, water exchange estimates work well for evapotranspiration, while assessment of its component fluxes (i.e. transpiration, evaporation) are still error prone (Talsma et al., 2018).

In particular simplifications in assessment schemes combined with insensitivity of RS proxies for complex water related mechanisms in the soil-plant-atmosphere system can partly explain observed biases and uncertainties in estimates of ecosystem functions (Dolman et al., 2014; Miralles et al., 2019). So-called plant-water relations act at different time scales and are highly sensitive to abiotic factors (e.g. soil water availability, atmospheric demand for water) and biotic factors (e.g. photosynthetic rates, stomatal conductance, plant structure). Knowledge of plant-water relations is, thus, critical to constrain estimates of ecosystem functioning under extreme conditions. A review by Damm et al. (2018) on the state of RS to assess plant-water relations indicates that this area is still dominated by empirical approaches to assess components of the complex water exchange between soil, plants and the atmosphere. Although mechanistic models exist (Bonan et al., 2014; Garcia-Tejera et al., 2017), they are rarely combined with RS data due to the complexity of required model parameters and missing sensitive observations.

Increasing maturity of RS technologies including measurements of sun-induced chlorophyll fluorescence (SIF) (Mohammed et al., 2019; Porcar-Castell et al., 2021) and multi-sensor concepts (Gerhards et al., 2016; Zarco-Tejada et al., 2012) opens additional opportunities to derive sensitive information and mechanistically assess plant-water relations (Jonard et al., 2020). SIF observations complement existing RS parameters and expand the range of RS accessible plant physiological processes towards ones acting at short temporal scales. In fact, it was recently found that SIF is sensitive to short term stomatal responses induced by water stress (Shan et al., 2019). Such developments complement traditional methods based on surface temperature, biochemical changes (i.e. decomposition of pigments, leaf water loss), mid-term acting structural adaptation, phenological responses, and ecosystem species composition (cf. Damm et al. (2018) for a review on this topic). However, the retrieval of SIF is delicate since superimposed by several other factors including counteracting physiological processes (i.e. non-photochemical quenching, NPQ) (Cendrero-Mateo et al., 2016), structural interferences (Li et al., 2019; Yang et al., 2019) and illumination effects (Damm et al., 2015; Yang et al., 2019). Besides SIF, the retrieval of common vegetation traits is also affected by illumination, structural and other effects (Barton and North, 2001; Damm et al., 2015; Myneni et al., 1995), which challenges their interpretation. Further, knowledge on causal relations between dynamics in plant response to water stress and required sensitivity of RS data are not fully exploited yet.

We hypothesize that retrieval uncertainties due to the complexity of common and new observations partly hide the inherent sensitivity of these observations for plant-water relations under water limited conditions. It is essential to disentangle unwanted sensitivities from targeted sensitivity of available RS parameter to finally provide mechanistic approaches for RS based assessments of plant-water relations. Further, it is important to understand specific temporal responses of RS indicators to soil water limitation. We therefore designed a soil water manipulation experiment in a maize field in Tuscany, Italy, with a particular focus on the sensitivity of physiological proxies (SIF and the photochemical reflectance index (PRI)), surface temperature (T_s), biochemical proxies (canopy water and chlorophyll content) for the early detection of water limitation. The field was equipped with several instruments to measure soil and plant water relations and environmental parameters, and we complemented these data with extensive biometric measurements and airborne RS observations. We assess diverse impacts of soil water limitation on plant hydraulic and growth parameters using in situ measurements. We then apply time series analysis to unravel the temporal sensitivity of various RS observations for increasing water limitation. We discuss and consolidate our results to suggest essential observations for robust assessments of the complex cascade of functional, biochemical and structural plant responses that evolve under increasing soil water limitation.

2. Methods

2.1. Test site and experimental design

The core experimental area of this study is a 220 × 320 m maize field (42°51′01.8"N 11°03′49.4″E, 10 m a.s.l.), located in a large agricultural region close to the city of Grosseto, Tuscany, Italy. The test site has a typical Mediterranean climate with hot and dry summers and mild winters. The maize field is equipped with a drip irrigation system, where the tubes are filled with water every two to three days for around 3 h. On average, a total amount of 6 mm of water per day is delivered independently of the natural precipitation regime, resulting in a soil moisture content of 20% per volume. On 13th June 2019, the irrigation tubes were removed from one sub-plot of 50x35m in the south of the field (orange box in Fig. 1). In situ measurements took place from 10 June to 24 June in the water-limited area and a well-watered area next to the treated canopy (orange and blue box in Fig. 1). Since canopy structure and observation/illumination geometry can influence the retrieval of RS parameters and cause differences between both investigated plant rows, we identified two other plots in the same plant rows to quantify the effect of these superimposing factors and facilitate the interpretation of our results (dark and light grey box in Fig. 1). Airborne data acquisition started on 16 June and lasted until 24 June. After the experiment, the irrigation was re-established in the water-limited canopy area.

2.2. In situ environmental and plant measurements

2.2.1. Environmental data

Canopy temperature and relative humidity were continuously measured above the canopy with a portable weather station. Soil water content in the first 25 cm of the soil was determined on 13, 16, 18, 20 and 22 of June using a portable Time Domain Reflectometry (TDR) probe. A FloX spectrometer system (jb-hyperspectral.com) was installed 3 m above the water-limited canopy area to measure irradiance and canopy reflected radiance every two minutes in high spectral resolution (i.e. 0.17 nm between 650 and 800 nm, 1.5 nm between 400 and 950 nm). We derived photosynthetic active radiation (PAR) by calculating the integral of the irradiance measurements between 400 and 700 nm.

2.2.2. Plant growth

Plant growth parameter were non-destructively collected in situ every two days on 11 marked plants per treatment. Plant height and steam diameter were measured on 11 June before the irrigation was stopped and from 16 to 28 of June. We calculated growth rates from

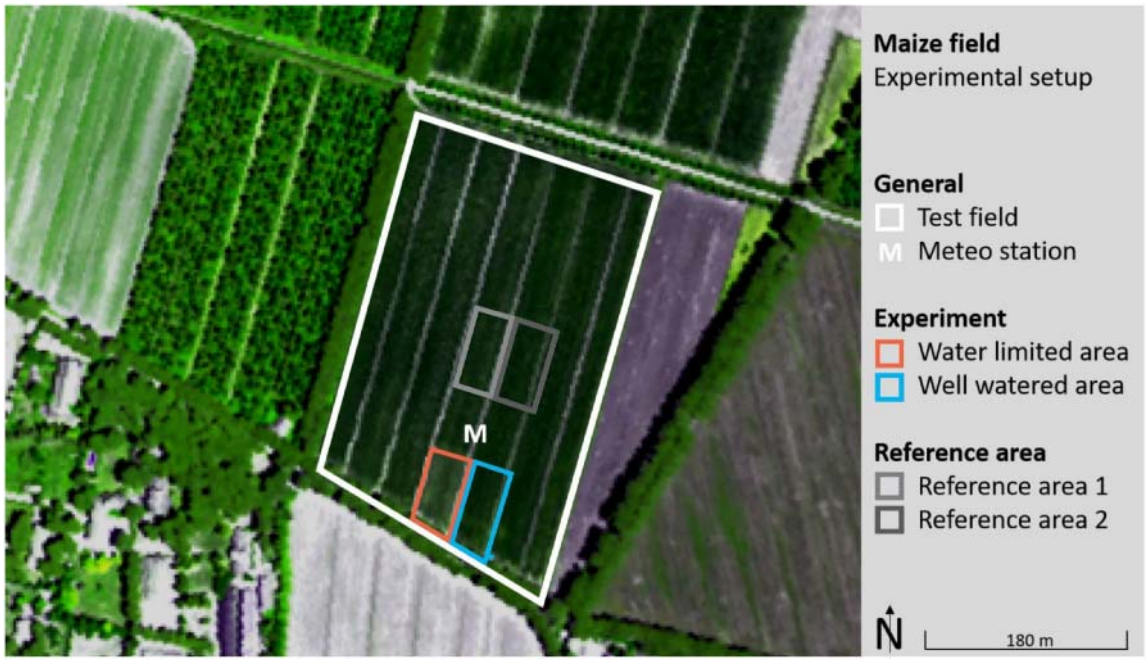

Fig. 1. Test site (white box) and experimental setup with the water-limited canopy (orange box) and the well-watered canopy (blue box), both equipped with in situ measurements. The grey marked areas are used to evaluate the temporal difference between plant rows due to superimposing structural and illumination / observational effects. The background image shows a false colour composite of HyPlant on 24 June 2019. (For interpretation of the references to colour in this figure legend, the reader is referred to the web version of this article.)

height measurements as difference between two adjacent observations per treatment.

2.2.3. Chlorophyll content

Variation in chlorophyll content was determined indirectly via measurements with a SPAD-502 chlorophyll meter (Konica-Minolta) on 11 marked plants per treatment. The SPAD instrument measures the difference of light transmission at two contrasting wavelengths differently affected by chlorophyll absorption. The resulting SPAD value requires an empirical conversion to effective chlorophyll content but in absence of such a function, we did not convert SPAD readings in units of chlorophyll content. Measurements started on 11 June before the irrigation was stopped and was continued every second day between 16 and 22 June.

2.2.4. Leaf water potential

Leaf water potential (ψ_l) was measured from 18 to 22 June on five individual maize plants that were randomly chosen in both the water-limited and well-watered canopy area. The upper fully expanded leaves were removed, stored in a plastic bag to avoid water losses (Turner and Long, 1980) and immediately measured. Leaf water potential was determined by means of a pressure chamber (PMS, Instrumentation Co. Corvallis, OR, USA) according to the Scholander et al. (1965) method. Leaves were measured between 10:00 and 15:30 on 18, 19, 20, and 21 June (mid-day measurements) and between 6:30 and 7:45 on 22 June (pre-dawn measurement).

2.2.5. Stomatal conductance

From 16 to 19 June, we measured leaf stomatal conductance (g_s) in mmol m^{-2} s^{-1} with a SC-1 Leaf Porometer (Decagon Devices, Inc., Pullman, WA, United States) during the day between 7:30 and 17:00. We obtained g_s for nine maize plants in both the water-limited area and the well-watered area. We took five measurements on the abaxial leaf side per maize plant and the measurements were distributed all around the plant stem to account for different leaf geometry and orientation.

2.2.6. Sap flow measurements

Canopy transpiration was measured by means of heat-balance sap-flow gauges (Peressotti and Ham, 1996), where heat is applied to the entire circumference of the stem encircled by a heating tape and the sap flow is obtained by measuring the difference in the fluxes of heat into and out of the heated section of the stem (Sakuratani, 1981). Ten gauges were installed on an equivalent number of plants in the irrigated and the non-irrigated plot and the fluxes were calculated at half-hour intervals from 8 June to 25 of June to obtain reliable estimates of the amount of water transpired.

2.3. Airborne spectroscopy in the optical domain

The main analysis of this paper is based on 42 flight lines acquired with the airborne imaging spectrometer HyPlant between 16 and 24 June (Table 1).

The HyPlant system consists of three pushbroom line scanners. Two of them share the same fore optic and form the DUAL module. This module quasi continuously samples the visible/near infrared (VNIR) and shortwave infrared (SWIR) spectral range (380–2500 nm) with a spectral resolution of 3.65 nm (VNIR) and 10.55 nm (SWIR). The third pushbroom line scanner, called FLUO, is able to record data in the spectral range between 670 and 780 nm with a spectral resolution of 0.28 nm (Rascher et al., 2015; Siegmann et al., 2019). While the DUAL

Table 1
Time of HyPlant flights during the experimental period in central European summer time (CEST).

Date	Morning (CEST)	Afternoon (CEST)
16 June	11:28, 11:32, 11:37, 11:41	14:11, 14:15, 14:19, 14:24
17 June	11:20, 11:24, 11:28, 11:33	
18 June	11:13, 11:17, 11:21, 11:26	14:22, 14:27, 14:32, 14:37
19 June	10:11, 10:19, 10:27, 10:34	13:15, 13:22, 13:30, 13:38
		16:11, 16:18, 16:26, 16:34
20 June		14:12, 14:16, 14:21, 14:25
23 June	11:09, 11:14, 11:18, 11:28	
24 June	11:13, 11:17	

module enables the retrieval of common vegetation parameter, i.e., canopy structure, pigment composition and other biochemical traits, the FLUO module facilitates the retrieval of SIF in both, the O_2-A and O_2-B absorption band. The flight height of 350 m resulted in a pixel size of 1 m. After a rigorous data pre-processing following the procedure described in Siegmann et al. (2019), we retrieved SIF and other remote sensing proxies indicative for the vegetation state.

2.3.1. SIF retrieval

Red and far-red SIF were quantified by exploiting the O_2-B and O_2-A absorption bands using and adapted Spectral Fitting technique (Meroni et al., 2010; Cogliati et al., 2015). The algorithm relies on forward simulations of at-sensor radiance spectra at the O_2 bands by means of coupled surface-atmosphere radiative transfer equations (Cogliati et al., 2019; Verhoef et al., 2018). The surface reflectance and fluorescence are modeled with simple parametric equations characterized by a spectrally smooth behaviour (i.e. polynomials for reflectance, peak-like functions for fluorescence). The physically based code *MODerate resolution atmospheric TRANsmission* 5 (MODTRAN-5) (Berk et al., 2005) is instead employed to calculate the atmospheric radiative transfer within the narrow windows corresponding to the O_2 bands. The exact atmospheric state is often unknown, causing slight uncertainties in the description of the atmospheric state and finally SIF retrieval uncertainties. We therefore used an image-based approach to optimize the parameterization of the atmospheric radiative model. In practice, the surface-sensor path length (i.e. determining the amount of oxygen absorption) was varied in MODTRAN-5 to analytically retrieved the effective path length that satisfies the condition of zero SIF for non-fluorescent targets. Instrument center wavelength and bandwidth were characterized with the SpecCal algorithm originally proposed by Meroni et al. (2010) and adapted for airborne data analysis. Resulting sensor characteristics are essential to convolve MODTRAN-5 based atmospheric transfer function. The retrieval of SIF within both O_2 bands is based on an iterative optimization algorithm that matches at-sensor radiance spectra measured with HyPlant and forward modeled using the coupled surface-atmosphere radiative transfer equations.

2.3.2. Other vegetation parameter

Based on the top-of-canopy reflectance derived from HyPlant DUAL data after atmospheric correction (Siegmann et al., 2019), the MERIS terrestrial chlorophyll index (MTCI) (Dash and Curran, 2004), Water Band Index (WBI) (Penuelas et al., 1993) and Photochemical Reflectance Index (PRI) (Gamon et al., 1992) were calculated to approximate canopy chlorophyll content, canopy water content, and non-photochemical quenching, respectively. The three reflectance indices were calculated as:

$$\mathrm{MTCI} = \frac{R_{754\pm4} - R_{709\pm5}}{R_{709\pm5} + R_{754\pm4}} \quad (1)$$

$$\mathrm{WBI} = \frac{R_{955-970}}{R_{890-905}} \quad (2)$$

$$\mathrm{PRI} = \frac{R_{570\pm2.5} - R_{531\pm2.5}}{R_{570\pm2.5} + R_{530\pm2.5}} \quad (3)$$

where R_λ correspond to the average reflectance of the HyPlant DUAL spectral bands. We used the average over the wavelength interval specified by the subscripts in Eqs. 1–3 to compensate for data noise.

2.4. Airborne thermal remote sensing

Along with the collection of HyPlant data, we acquired thermal data using the TASI-600 spectroradiometer. TASI is a pushbroom line scanner measuring in the longwave infrared (LWIR) spectral region between 8′000 to 11′500 nm in 32 spectral bands (Itres Research Ltd). The flight height of 350 m resulted in a spatial resolution of 1.8 m. Acquired data were processed by a standard processing chain described in Hanus et al. (2016), further details can be also found under (http://olc.czechglobe.cz/en/processing/tasi-data-processing/). The standard processing includes a radiometric correction using the RadCor software (Itres Research Ltd) and, in absence of calibrated black body scans, laboratory determined calibration coefficients. Afterwards, an atmospheric correction was applied to compensate atmospheric up and downwelling radiance and atmospheric transmissivity and finally retrieve land surface temperature (T_S).

2.5. Data normalization at airborne level

We applied two data normalization strategies to compensate canopy structural and illumination effects that often superimpose dynamics in retrieved SIF and other vegetation parameters. A first data normalization only acted in the temporal domain. We calculated the difference between investigated RS parameter (P) at a certain point in time and the mean of the RS parameter obtained from the first four airborne data acquisitions of the campaign in the morning of 16 June (e.g. P^{16}) as:

$$\Delta P = P - P^{16} \quad (4)$$

The resulting time series of ΔP represents the increment of individual RS parameter considering the first four observations (16 June) in physical units. It must be noted that the first flight took place three days after the irrigation was stopped (13 June) but both the water-limited and the well watered canopy areas were still in the same state with no signs of soil water limitation.

The second data normalization acted in the spatial and temporal domain. We calculated the normalized difference of a RS parameter for the water-limited canopy (P_{EXP}) considering the well-watered canopy as reference (P_{REF}) (orange and blue area in Fig. 1) for a given point in time ($P_{EXP\text{-}REF}$). Further, we calculated the same normalized difference considering two reference areas in the same rows but not affected by the experiment, while the canopy in sam row as the water-limited canopy was used as (P_{EXP}) and the other one as (P_{REF}) (bright grey and grey area in Fig. 1).

$$P_{EXP-REF} = \frac{P_{EXP} - P_{REF}}{P_{REF}} \bullet 100 \quad (5)$$

Resulting spatially normalized $P_{EXP\text{-}REF}$ values were then related to the mean of the first four observations of 16 June ($P_{EXP-REF}^{16}$) to calculate a time series of increments of spatially normalized differences ($\Delta P_{EXP\text{-}REF}$) considering the first observation (16 June) as:

$$\Delta P_{EXP-REF} = P_{EXP-REF} - P_{EXP-REF}^{16} \quad (6)$$

Resulting $\Delta P_{EXP\text{-}REF}$ values for SIF, MTCI, PRI, WBI, T_S are supposed to normalize structural and related illumination effects caused by different observation times and view angles.

2.6. Statistics

We used two statistical measures to evaluate the effect and reliability of the applied water limitation on the response of plants as approximated by the various RS parameters, including the 95% confidence intervals assuming a z-distribution and the effect size using *Cohen's d* by taking the standard deviation of the well-watered canopy into account. Since the maize field was covered with many observations (pixels), we selected every tenth pixel per region of interest (cf. Fig. 1) to minimize the problem of spatial (e.g. environmental factors) and technical autocorrelation (e.g. pixel-cross talk), and to reduce the number of observations.

3. Results

3.1. Environmental parameter

During the observational period, weather conditions were good with five almost cloud free days, six days with scattered clouds and one day with overcast conditions (22 June), while PAR reached up to 400 W m^{-2} on partly scattered days (Fig. 2*A*). Air temperature ranged between 11.7 and 37.1 °C with a mean of 24.3 °C (Fig. 2*B*). Relative humidity ranged between 21.7% and 93.9% with a mean value of 60.5% (Fig. 2*C*). The induced irrigation-stop caused an immediate drop of soil water content, reaching a reduction of 65% at the end of the experiment (Fig. 2*D*).

3.2. Impact of soil water limitation on plant-water relations from an in situ perspective

3.2.1. Plant growth

We found a reduced growth rate between the water-limited and the well-watered canopy. Both canopies had similar stem diameters at the beginning of the experiment (26.5–26.8 mm), while plants in the water limited canopy showed a significantly reduced increase of the stem diameter compared to plants in the well-watered canopy. Already on 16 June, notable differences were observed that reached 10% at the end of the experiment (31.8 mm for the well-watered canopy, 28.9 mm for the water-limited canopy) (Fig. 3*A*). Concerning canopy height, plants in both canopies started with different heights (i.e. 82 cm for the well-watered canopy, 75 cm for the water limited canopy, Fig. 3*B*). Both canopies showed a height increase, with plants of the water-limited area lagging behind and reaching a 22% difference at the end of the experiment (i.e. 1.7 m of the well-watered canopy and 1.3 m of the water-limited canopy (Fig. 3*B*). The growth rates for the well-watered canopy continuously increased from 2 cm/day to 8.3 cm/day on 28 June (Fig. 3*D*). Growth rates for the watered-limited plants increased from 1 cm/day to and 4.5 cm/day on 22 June and even decreased until 25 June (2 cm/day) but showed a substantial increase towards the end of the experiment (7 cm/day) when the water-limited canopy was again irrigated.

3.2.2. Leaf chlorophyll content

SPAD based estimates of the leaf chlorophyll content indicate that both treatments started at a comparable level (i.e. 50.7 and 51.1 SPAD values) and showed a notable difference already on 16 June. The SPAD value slightly decreased for the water-limited plants (reaching 49.7 on 22 June), while SPAD values increased for the well-watered canopy (52.5 on 22 June) (Fig. 3*C*).

3.2.3. Leaf water potential

ψ_l measurements were started on 18 June, 5 days after the irrigation was stopped and soil water content already droped by 52%, and were lower in water-limited canopy (−12.13 MPa to −13.83 MPa) compared to the well-watered canopy (−9.27 MPa to −10.48 MPa) (Fig. A1*A*). Pre-dawn measurements made on 22 June, 9 days after the experiment started, indicate manifested water limitation in terms of reduced ψ_l (i.e. -9.17 MPa), while the well-watered canopy has a higher ψ_l (−5.2 MPa) (grey marked area in Fig. A1*A*).

3.2.4. SAP flow

SAP flow shows a large dynamic at a diurnal time scale and across the experiment (Fig. A1*B*). A typical diurnal pattern with highest values around noon-time (0.5–0.8 mm h^{-1}) is overlaid with some scatter caused by environmental factors (e.g. varying net radiation, wind, temperature). Diurnal differences between the water-limited and the well-watered canopy are particularly visible before noon with a reduced SAP flow of the water limited canopy from 13 June until 23 June. After the irrigation was re-established, SAP flow rates of the water-limited canopy substantially increased and even exceeded the rated of the well-watered canopy, reaching maximum values of 0.8 mm h^{-1}. Daily aggregated SAP flow started at a similar level on 10 June (3.5 mm day^{-1}), while the daily rates for the well-watered canopy were constantly larger compared to the water-limited canopy with an increasing difference until 22 June. After the cloudy day on 22 June with some rainfall and re-establishing the irrigation afterwards, daily rates of the water-limited canopy even exceeded the one of the well-watered canopy and reached values of 6 mm day^{-1}. (Fig. A1*B*).

3.2.5. Stomatal conductance

g_s measurements started on 16 June, three days after irrigation was stopped. Acquired data are scattered and less conclusive (Fig. A2). In general for both, the water-limited and the well-watered canopy, we observe an increase of g_s from the morning (50–90 mmol m^{-2} s^{-1}) to noon time (80–140 mmol m^{-2} s^{-1}). Concerning diurnal changes between both treatments, our measurements tend to show that the slope of a fitted linear model representing diurnal dynamics stays relatively constant for all days in the well-watered canopy (i.e. slope between 1.3 and 6.2), and declines from 5.6 (16 June) to −0.2-1.7 (18 and 19 June) in the water-limited canopy (Fig. A2). The water-limited canopy shows a

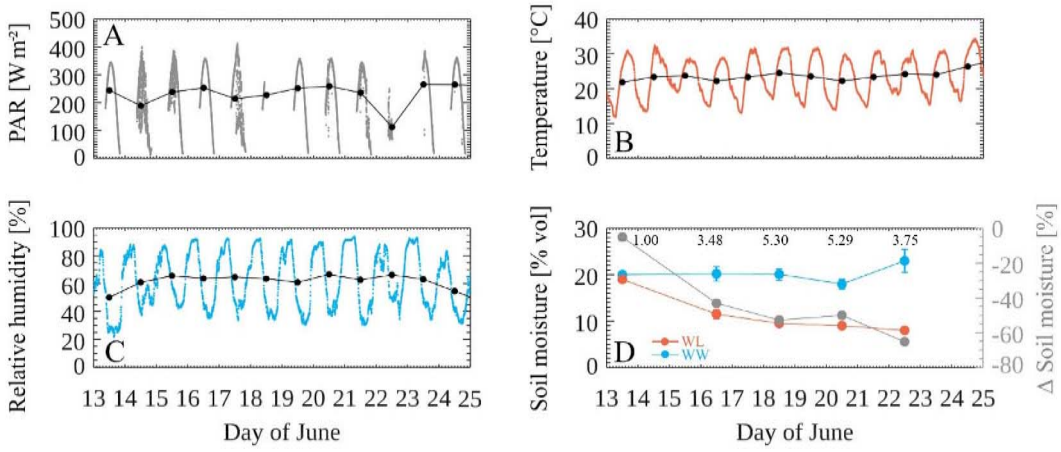

Fig. 2. Overview of environmental factors during the duration of the experiment from 13 to 25 June 2019. A: Photosynthetic active radiation (PAR). B: Air temperature at 2 m height. C: Relative humidity at 2 m height. D: Volumetric soil water content in the upper 25 cm of the water-limited (WL) area (orange), the well-watered (WW) area (blue) and the percent difference between both curves (grey). The black dots in A-C represent the mean value per day. Error bars indicate the 95% confidence interval and numbers the effect size (Cohen's d). (For interpretation of the references to colour in this figure legend, the reader is referred to the web version of this article.)

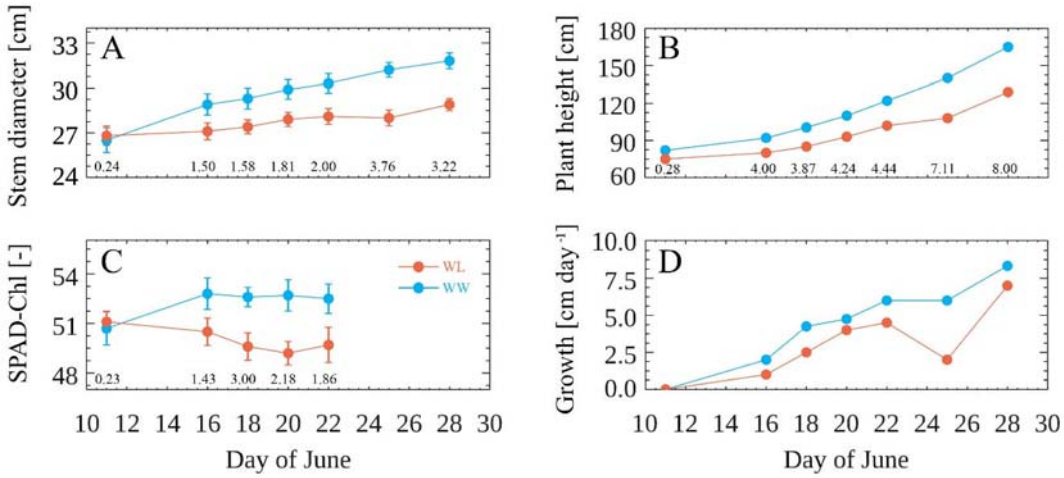

Fig. 3. Development of structural, biochemical and growth parameters of the water-limited (WL) area (orange) and the well-watered (WW) area (blue). A: Stem diameter. B: Plant height. C: SPAD based leaf chlorophyll content. D: Growth rate representing the height difference between two adjacent days. Error bars indicate the 95% confidence interval and numbers the effect size (Cohen's d). (For interpretation of the references to colour in this figure legend, the reader is referred to the web version of this article.)

decline of g_s in the late afternoon (mean g_s decreases from 140 to 70 mmol m^{-2} s^{-1} between 16 to 19 June), while the well-watered canopy shows a less varying mean g_s ranging between 95 and 125 mmol m^{-2} s^{-1} from 16 to 19 June (Fig. A2).

3.3. Temporal dynamics of plant-water relations from an airborne RS perspective

Investigated RS parameter red and far-red SIF, vegetation indices (i.e. PRI, MTCI, WBI) and Ts show diverse temporal responses in accordance to evolving soil water limitation (Fig. 4).

3.3.1. Fast changing remote sensing parameters: SIF_{760} and SIF_{685}

Compared to the first day of airborne measurements on 16 June, ΔSIF_{685} for the well-watered and the water-limited area at 11:00 continuously decrease and are lowered by around 0.32 and 0.18 mW m^{-2} nm^{-1} sr^{-1} on 24 June respectively (Fig. 4*A*). On 19 June, ΔSIF_{685} shows a local minima of around −0.45 mW m^{-2} nm^{-1} sr^{-1} for both areas since observations took place around one hour earlier compared to the other days. The normalized $\Delta SIF_{EXP-REF}^{685}$ values indicate a rapid increase of SIF_{685} of around 5.6–9.8% in the water-limited canopy compared to the well-watered canopy in the morning which stays at this level until 24 June (Fig. 4*B*). $\Delta SIF_{EXP-REF}^{685}$ of the reference plots indicate in average smaller SIF_{685} values for the plant row of the water-limited canopy compared to the other row but differences fluctuate around zero.

ΔSIF_{760} of the well-watered canopy increases in the morning by 0.43 mW m^{-2} nm^{-1} sr^{-1} from 16 to 24 June. ΔSIF_{760} of the water-limited canopy varies at the end of the experiment with increased values between 0.09 and 0.25 mW m^{-2} nm^{-1} sr^{-1} (Fig. 4*C*). Normalized $\Delta SIF_{EXP-REF}^{760}$ values show a highly interesting pattern. $\Delta SIF_{EXP-REF}^{760}$ of the water-limited canopy first increases compared to the well-watered canopy from 16 June to 18 June (11.9%) and then starts decreasing until 24 June (−7.7%) (Fig. 4*D*). The first increase is not visible for the reference canopies that exhibit in the first four days around 5% smaller SIF_{760} values in the plant row of the water-limited canopy compared to the plant row with the well-watered canopy, followed by a 7.9% increase of $\Delta SIF_{EXP-REF}^{760}$ towards 24 June.

3.3.2. Moderately changing remote sensing parameters: T_S, PRI, MTCI, WBI

ΔT_S values also show a slight but continuous increase in the morning for both treatments on the first two days (between 0.45 and 0.9 °C). On 19 June, ΔT_S declines (−0.76 to −1.0 °C) due to earlier data acquisition. The water-limited canopy eventually reaches an increased temperature of 3.5 °C on 24 June, while the well-watered one shows a temperature increase on 24 June of 1.2 °C (Fig. 4*E*). The normalized time series $\Delta Ts_{EXP\text{-}REF}$ indicates continuously increasing temperatures in the water-limited canopy, reaching 7.1% higher values compared to the well-watered canopy at the end of the experiment (Fig. 4*F*). $\Delta Ts_{EXP\text{-}REF}$ for the reference canopies is slightly decreasing until June 24 (−2.2%).

ΔPRI, indicative for NPQ, shows a decreasing trend between 16 and 24 June in the morning, while PRI values for the well-watered canopy show a larger decline compared to the water-limited canopy. The ΔPRI time series also shows discontinuity for both treatments (e.g. increasing values on 23 June, Fig. 4*G*). Normalized $\Delta PRI_{EXP\text{-}REF}$ values indicate a continuous increase of PRI for the water-limited canopy compared to the well-watered canopy, reaching 20.4% higher values on 24 June (Fig. 4*H*). The $\Delta PRI_{EXP\text{-}REF}$ values of the reference canopies indicate that PRI of both plant rows does not largely change from 16 to 24 June (−3.4 to 2.7%).

MTCI represents the canopy chlorophyll content. Retrieved ΔMTCI values show a continuous increase for both the water-limited and the well-watered and canopy until 19 June, followed by continuous increase of MTCI for the well-watered canopy until 24 June and a slight decline of MTCI for the water-limited canopy until 24 June (Fig. 4*I*). The normalized $\Delta MTCI_{EXP\text{-}REF}$ time series clearly shows that the water-limited canopy is affected by growth limitation. MTCI values stay constant until 19 June (change <1.5%) and then decline towards 24 June (−13.8%) (Fig. 4*J*). The $\Delta MTCI_{EXP\text{-}REF}$ values of the reference canopies indicate that MTCI of both plant rows does not notably change from 16 to 24 June (−0.02 to 3.0%).

ΔWBI values, indicative for the inverse of canopy water content, constantly decrease between 16 and 24 June for both canopies. The time series shows some discontinuity for both treatments (e.g. slight intermediate increases on 18 and 23 June) (Fig. 4*K*). Normalized $\Delta WBI_{EXP\text{-}REF}$ values confirm that the canopy water content does not notably change between the water-limited and the well-watered canopies (−0.57 to 0.69%). The $\Delta WBI_{EXP\text{-}REF}$ values of the reference canopies indicate also almost no WBI differences between both plant rows from 16 to 24 June (up to −1.5%, Fig. 4*L*).

3.4. Spatio-temporal dynamics of plant-water relations

The spatial representation of changes in normalized airborne RS parameters (i.e. $\Delta P_{EXP\text{-}REF}$) provides an additional and confirming

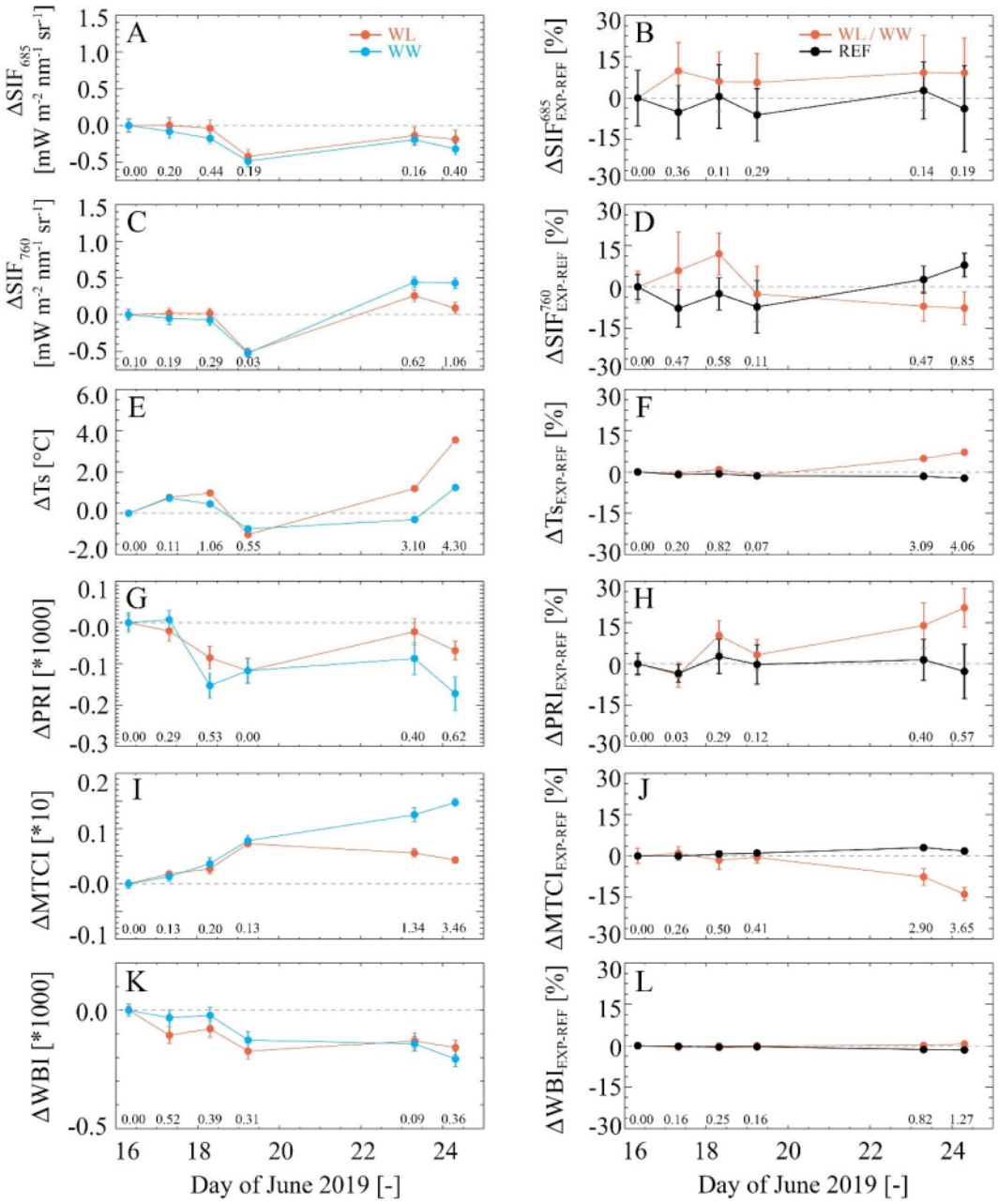

Fig. 4. Changes of remote sensing (RS) parameter during the water manipulation experiment in a maize canopy between 16 and 24 June 2019 acquired in the morning (10–11:30 CEST). Left column: Shown changes represented the difference of a certain RS parameter (P) compared to the first observation (16 June) in parameter units (ΔP) for the water-limited field (orange) and well-watered field (blue). From top to bottom: red sun-induced chlorophyll fluorescence (SIF685), far-red SIF (SIF760), surface temperature (Ts), photochemical reflectance index (PRI), MERIS terrestrial chlorophyll index (MTCI), and water band index (WBI). Right column: percentage changes representing the relative difference between the water-limited and the well-watered area (orange), normalized considering the percentage change of the first day (16 June) ($\Delta P_{EXP\text{-}REF}$). The black line shows the normalized percent changes of two reference areas in the same plant rows not affected by the water-limitation experiment. Error bars indicate the 95% confidence interval and numbers the effect size (Cohen's d). (For interpretation of the references to colour in this figure legend, the reader is referred to the web version of this article.)

perspective on trends explained in the previous section 3.3. Fig. 5 shows the maize field under investigation and highlights the relevant canopy areas.

$\Delta SIF_{EXP-REF}^{760}$ is rather noisy but one can recognize increased $\Delta SIF_{EXP-REF}^{760}$ values in the water-limited area, showing higher values on June 17 and 18 compared to the well-watered area. At the end of the campaign, $\Delta SIF_{EXP-REF}^{760}$ substantially decreases in the water-limited area but remains constant for the other regions. $\Delta SIF_{EXP-REF}^{685}$ is also rather noisy but no differences between both treatments are visible. $\Delta PRI_{EXP\text{-}REF}$ and $\Delta Ts_{EXP\text{-}REF}$ show an increasing contrast between well-limited and well-watered canopy starting on 18 June, while a notable difference between the water-limited and the well-watered canopy appears on 24 June. For $\Delta MTCI_{EXP\text{-}REF}$ and $\Delta WBI_{EXP\text{-}REF}$ a reduction of values in the water-limited area appears later than 18 June but is well visible on 24 June.

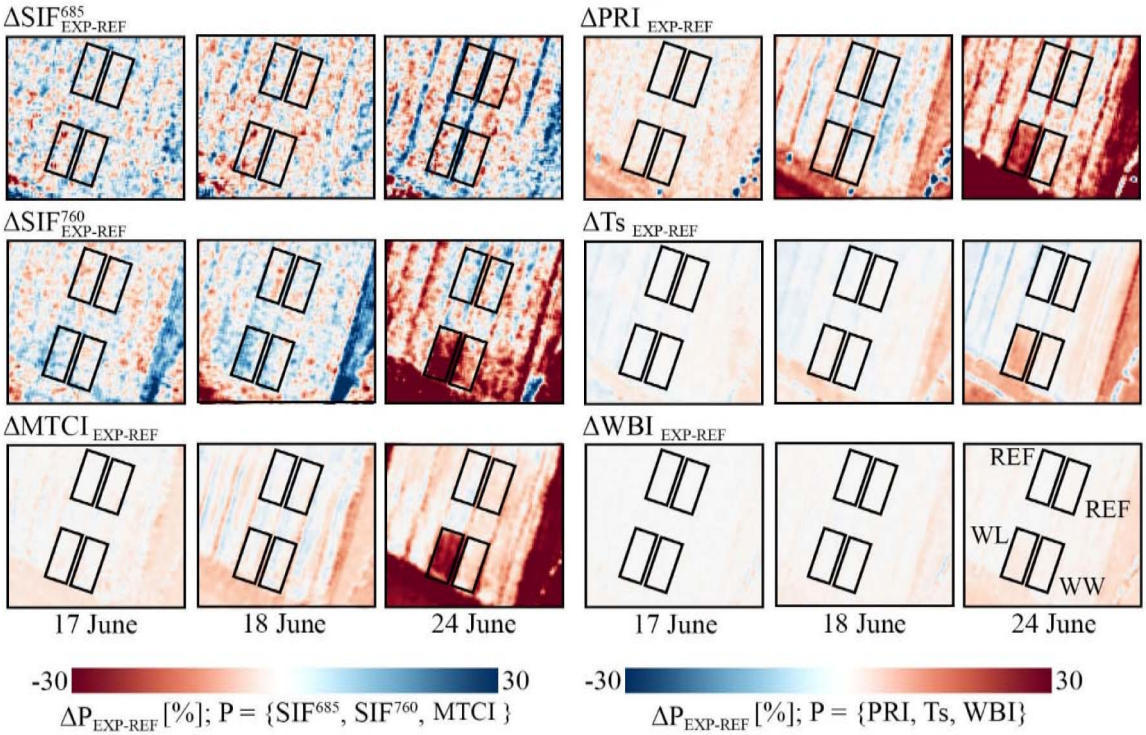

Fig. 5. Response of remote sensing (RS) parameter to evolving water-limitation in a corn canopy one day (17 June), two days (18 June) and eight days after start of flight experiment (24 June). The boxes indicate the locations of the differently treated areas of the experiment, i.e. water-limited (WL), well-watered (WW) and the two reference areas (REF). Please note that the colour scheme changes between RS parameters to enable an intuitive colour representation with red indicating a negative effect and blue a positive effect. (For interpretation of the references to colour in this figure legend, the reader is referred to the web version of this article.)

4. Discussion

4.1. Sensitivity of normalized remote sensing parameters for evolving soil water-limitation

We observed specific responses of normalized RS parameter to water-limitation that differ in their temporal dynamics and amplitude. This expected behaviour is caused by the sensitivity of individual RS parameters for specific plant adaptation mechanisms, including functional and biochemical/structural changes to water limitation (cf. Damm et al. (2018) for a review on this topic). Highly interesting is the observed morning double response of normalized SIF_{760} ($\Delta SIF_{EXP-REF}^{760}$) with first a short-term increase with increasing water-limitation, followed by a longer-term decrease under sustained water-limitation (cf. Figs. 4-5). Further, SIF_{685} ($\Delta SIF_{EXP-REF}^{685}$) showed an immediate increase but no reduction over time.

In fact, three to five days after the experiment started (16–18 June), soil moisture content was already reduced by 43% and 52% (Fig. 2*D*) and first signs of reduced SAP flow in the water-limited canopy in the morning hours were visible (Fig. A1*B*). In situ growth parameters already indicate a slight separation of the water-limited and well-watered canopy with even slightly reduced SPAD based leaf chlorophyll and growth rates for the water-limited canopy. An increase of SIF_{760} and SIF_{685} in the water-limited canopy compared to the well-watered canopy under these conditions where already a slight reduction of SIF due to the lower chlorophyll content could be expected is likely driven by physiology. We also calculated the NIRv that was introduced as RS proxy sensitive for structural variation of SIF (Badgley et al., 2017; Zeng et al., 2022). The $\Delta NIRv_{EXP-REF}$) time series shows only small differences in the first days between the well-watered and water limited canopies and the reference plots (2.8 and 4.0% respectively), indicating no structural difference between both, the well-watered and the water-limited canopy that could explain the shorter dynamics in SIF (Fig. A3*B*, Fig. A5*B*). Dynamics in red and green reflectance was analysed and we found fast and continuous responses of $\Delta R_{GREEN\ EXP-REF}$ and $\Delta R_{RED\ EXP-REF}$ starting on 18 June that cannot explain the fast increase of $\Delta SIF_{EXP-REF}^{760}$ on 17 June and the decline after 19 June (Fig. A3*F*, A3*H*). Other RS derived parameters support that plants could have reacted physiologically to the evolving water-limitation. Slightly higher $\Delta Ts_{EXP-REF}$ in the water-limited field compared to the well-watered field already visible in the morning but even more pronounced in the afternoon (Fig. A4*F*) could indicate a partly stomatal closure that possibly inhibits PS and thus increases chances of SIF emission. $\Delta PRI_{EXP-REF}$, representing the regulation of NPQ, is similar in the morning for the water-limited and well-watered canopy until 17 June and increases afterwards, indicating that NPQ in water-limited canopy does not reach a critical level to quench notably more electrons from the light reaction compared to the well-watered canopy at least until 17 June.

After eleven days after the experiment started (22 June), soil moisture content of the water-limited field decreased by 65% compared to the well-watered canopy. Growth sensitive RS parameters show a relevant reduction ($\Delta MTCI_{EXP-REF}$ and $\Delta WBI_{EXP-REF}$), confirmed by in situ observations of growth parameters. The decline of $\Delta SIF_{EXP-REF}^{760}$ (lower SIF_{760} in the water-limited field compared to the well-watered field) after 19 June is possibly determined by structural changes (i.e. lower canopy chlorophyll in the water-limited treatment) and physiological effects. The structural sensitivity is confirmed by the lowered $\Delta NIRv_{EXP-REF}$ for the experimental canopies (−5.0%) and the parallel increase for the reference canopies (5.7%) (Fig. A3*B*). Further, the increasing $\Delta Ts_{EXP-REF}$ in the morning and afternoon indicates higher stomatal closure in the water-limited canopy, while increasing $\Delta PRI_{EXP-REF}$ in the water-limited area compared to the well-watered area indicates substantial NPQ that causes a stagnation or even lower SIF_{760} in the water-limited canopy compared to the well-watered canopy.

Earlier studies (van der Tol et al., 2009; Van Wittenberghe et al.,

2021) demonstrate at leaf level that SIF together with NPQ increases with environmental stress. The modelling study by van der Tol et al. (2009) additionally indicates a NPQ threshold causing a stagnation or even decreases of SIF when NPQ becomes the dominant pathway of photons (cf. Fig. 3a in (van der Tol et al., 2009). At coarser canopy level, several studies indicate a decrease of SIF_{760} with environmental stress (Sun et al., 2015; Yoshida et al., 2015). Both results seem contradicting but can be explained by the complex interplay of physiological and structural plant response to drought that act at different time scales. The theoretically known double response of SIF_{760} under evolving stress is, to our knowledge, now for the first time shown in an airborne experiment.

Concerning SIF_{685}, we observed increase of $\Delta SIF_{EXP-REF}^{685}$ in the water-limited canopy during the entire period. It is known that red SIF is re-absorbed by chlorophyll and the observed behaviour of $\Delta SIF_{EXP-REF}^{685}$ is likely a complex interplay of a longer-term structural response and physiological SIF_{685} changes that seem to keep in balance.

4.2. Limitation of this study and ways forward

Results obtained in this study correspond to theory discussed in literature and findings from airborne level are supported by detailed in situ measurements. Nevertheless, some limitations of our experimental setting must be noted to better judge reliability and representativeness of obtained results.

One limitation is that we present results from a single maize field that was measured once without replicates. This certainly asks for other studies to repeat such an experiment ideally at a variety of different crops and environmental settings. Although a comprehensive set of in situ observations was available, it is not complete. Collected data are sufficient to reveal a clear plant growth response for increasing water-limitation but more supportive measurements would be helpful for data interpretation and transferability of results. Particularly interesting would be eddy flux measurements of evapotranspiration and leaf physiological information including NPQ and g_s obtained from leaf gas chamber measurements. Further, more detailed soil water data such as soil water content, soil water holding capacity and field capacity would be important to quantify plant available water.

Besides SIF, we used simple retrieval approaches to quantify plant parameter from airborne data (i.e. vegetation indices) and RS data were acquired under slightly different observation times in the morning (10:15–11:30) and afternoon (13:30–15:30). It is well known that the retrieval of RS plant parameters must account for various superimposing factors, including illumination effects (Damm et al., 2015; Fawcett et al., 2018; Kückenbrink et al., 2019), atmospheric disturbances (Cendrero-Mateo et al., 2019; Guanter et al., 2010), canopy structure (Feng et al., 2002) with its related reflectance anisotropy (Weyermann et al., 2014), and instrumental effects (Damm et al., 2011; Hueni et al., 2017). Since the compensation of these disturbing effects if often less reliable than required, small artefacts in retrieved RS parameter remain. Furthermore, RS parameter represent highly dynamic traits (e.g. SIF, Ts) that change during the day, while slightly different observation times immediately complicate the interpretation of observed RS parameter dynamics. Our results indicate that revealing subtle canopy responses such as the double SIF_{760} response from original time series is difficult due to imperfections of RS parameter retrieval schemes.

We consequently applied a rigorous spatio-temporal data normalization to compensate RS parameter variation caused by above superimposing effects. Our results successfully demonstrate that most of these superimposing effects can be compensated with such normalization strategies (cf. differences between ΔP and normalized $\Delta P_{EXP\text{-}REF}$ trends in Fig. 4), which is in agreement with other studies (Zarco-Tejada et al., 2012). The implementation of spatio-temporal normalization strategies is not straightforward due to missing references. Our experiment provided important insight on the severity of these superimposing effects and clearly indicates the need for an optimized planning of combined field and airborne experiments. Concerning environmental monitoring at larger scales, temporal normalization and rigorous data filtering would be essential to avoid misinterpretation of data.

Our study provides further evidence that the RS based assessment of plant responses to water-limitation is complex. Approximating plant stress using multiple RS parameter sensitive for involved processes that act at different temporal scales should be preferred over the use of single parameter. Particularly sensitive, independent and complementary proxies including SIF_{760}, Ts, NPQ (via PRI or more sophisticated approaches), and growth sensitive parameter (leaf pigments and water content, LAI) are of high interest as also discussed in previous research (Damm et al., 2018; Gerhards et al., 2016).

5. Conclusions

New RS technology opens various pathways to assess plant-water relation across ecological relevant scales but the complexity of environmental stress related plant responses still poses a substantial challenge. Our experimental findings confirm theoretical knowledge on the variety of physiological plant reactions following evolving soil water-limitation and their respective temporal dynamics (i.e. SIF representing fast changing adaptation, followed by PRI (as proxy for NPQ), Ts, MTCI (as proxy for canopy chlorophyll content) and WBI (as proxy for leaf water content)). We conclude that canopy measured SIF_{760} shows a highly complex response to emerging soil water-limitation, with a mainly physiology caused short-term increase compared to its normal, followed by a decrease due to biochemical and structural effects. This theoretically known behaviour was here for the first time shown at canopy scale using airborne data. We conclude that time series of spectroscopy images, rather than point measurements and a rigorous data normalization is key to compensate for the various factors causing dynamics in observed RS parameter. Particularly effects caused by changing illumination and structure substantially superimpose dynamics in retrieved RS parameter that tend to mask subtle plant responses. We suggest to substantially invest in research to exploit multi-data approaches for a consistent observation of plant information representing first and second order responses of plant-water relations. We consider such approaches to provide most robust and mechanistic insight on environmental change effects on ecosystem functioning.

Credit author statement

A.D., R.C., F.M., U.R., D.S. conceptualized the experiment; A.D. implemented the data analysis; S.C., P.R., B.S. and J.H. processed airborne data and documented them; L.F., J.S., A.G., L.G., A.P., J.S. acquired, processed and described the field data; A.D. prepared an advanced draft of the manuscript with contributions from S.C., R.C., L. F., A.G., L.G., B.S., J.S., and F.M. All co-authors reviewed and edited the manuscript draft.

Data sharing and accessibility

The data that support the findings of this study are available from the corresponding author upon reasonable request and will be soon available via the campaign data site of ESA.

Declaration of Competing Interest

The authors declare that they have no known competing financial interests or personal relationships that could have appeared to influence the work reported in this paper.

Acknowledgements

Airborne data acquisition and parts of the data analysis was financed by the European Space Agency (ESA) in the frame of the FLEXSense

campaign (ESA Contract No. 4000125402/18/NL/NA) and the Photoproxy campaign (ESA contract No. 4000125731/19/NL/LF). We are grateful to the anonymous reviewers for providing excellent and highly constructive comments to improve this manuscript.

Appendix A

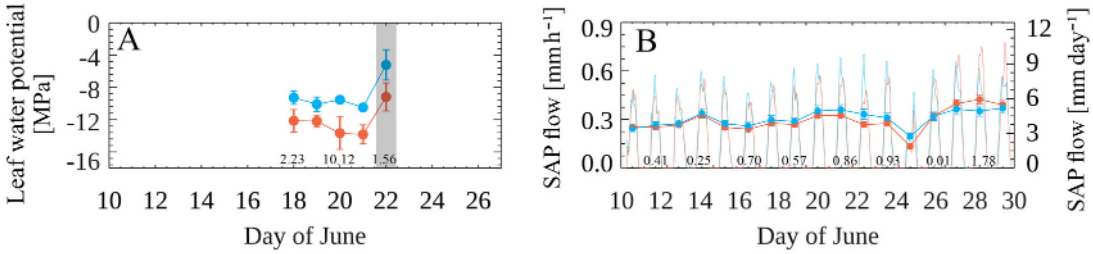

Fig. A1. Left: Mean Leaf water potential (in MPa) of well-watered (blue) and water-limited (orange) corn leaves around noon time. The measurement on 22 June represents pre-dawn conditions. Error bars indicate the 95% confidence interval. Right: Mean diurnal cycles of sap flow measurement of ten corn plants in the well watered canopy (blue) and ten in the the water-limited area (orange). Dots represent daily mean values. Error bars indicate the 95% confidence interval for this period. Numbers in both panels show the effect size (Cohen's d). (For interpretation of the references to colour in this figure legend, the reader is referred to the web version of this article.)

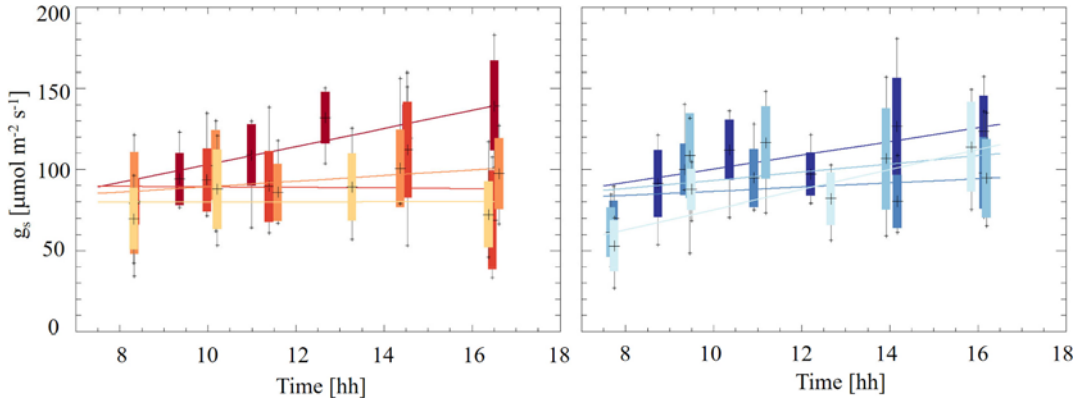

Fig. A2. Stomatal conductance (g_s) between water-limited canopy (left) and well-watered canopy (right). Boxes indicate the mean (black cross), standard deviation (extend of the box) and extreme values (black vertical lines) of 30 measurements on nine plants within 30 min. The lines indicate a linear model fitted to mean g_s values per diurnal cycle. Colours indicate the time of the experiment, ranging from dark red and blue (16 June) to yellow and bright blue (19 June). (For interpretation of the references to colour in this figure legend, the reader is referred to the web version of this article.)

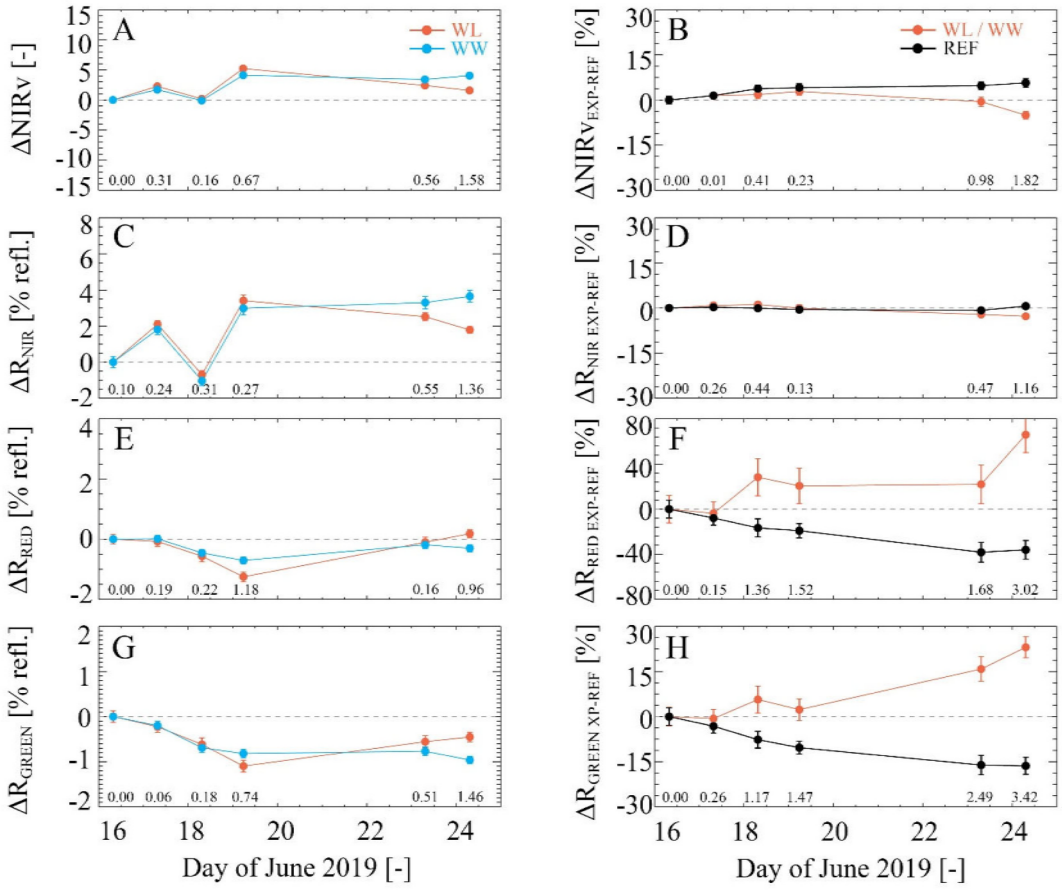

Fig. A3. Changes of the structure sensitive vegetation index NIRv and green, red and NIR reflectance during the water manipulation experiment in a maize canopy between 16 and 24 June 2019 acquired in the morning (10:00–11:30 CEST). Left column: Shown changes represented the difference of a certain RS parameter (P) compared to the first observation (16 June) in parameter units (ΔP) for the water-limited field (orange) and well-watered field (blue). Right column: percentage changes representing the relative difference between the water-limited and the well-watered area (orange), normalized considering the percentage change of the first day (16 June) ($\Delta P_{EXP\text{-}REF}$). The black line shows the normalized percent changes of two reference areas in the same plant rows not affected by the water-limitation experiment. Error bars indicate the 95% confidence interval and numbers the effect size (Cohen's d). (For interpretation of the references to colour in this figure legend, the reader is referred to the web version of this article.)

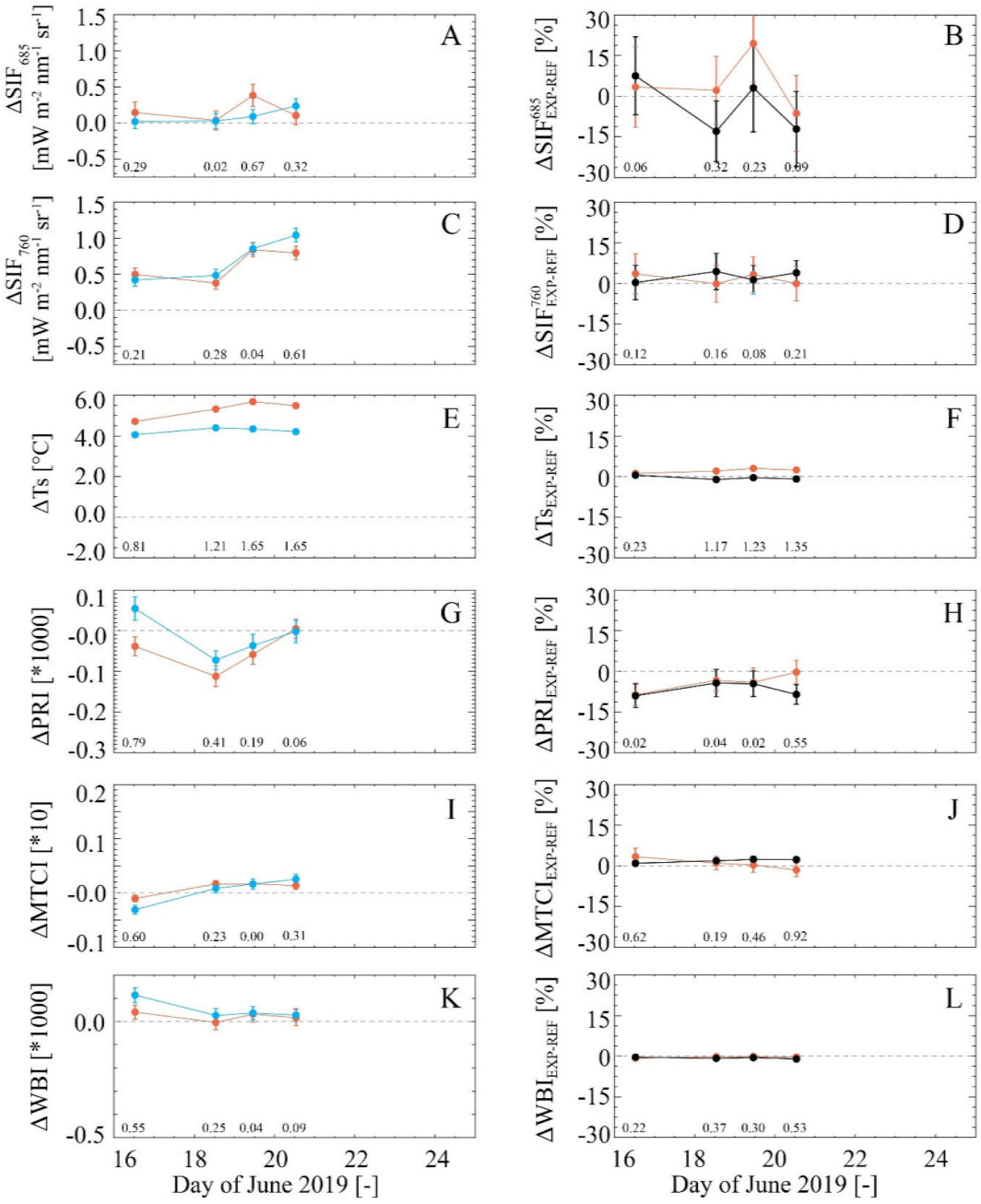

Fig. A4. Changes of remote sensing (RS) parameter during the water manipulation experiment in a maize canopy between 16 and 24 June 2019 acquired in the afternoon (13:30–14:30 CEST). Left column: Shown changes represented the difference of a certain RS parameter (P) compared to the first observation (16 June) in parameter units (ΔP) for the water-limited field (orange) and well-watered field (blue). From top to bottom: red sun-induced chlorophyll fluorescence (SIF685), far-red SIF (SIF760), surface temperature (Ts), photochemical reflectance index (PRI), MERIS terrestrial chlorophyll index (MTCI), and water band index (WBI). Right column: percentage changes representing the relative difference between the water-limited and the well-watered area (orange), normalized considering the percentage change of the first day (16 June) ($\Delta P_{EXP\text{-}REF}$). The black line shows the normalized percent changes of two reference areas in the same plant rows not affected by the water-limitation experiment. Error bars indicate the 95% confidence interval and numbers the effect size (Cohen's d). (For interpretation of the references to colour in this figure legend, the reader is referred to the web version of this article.)

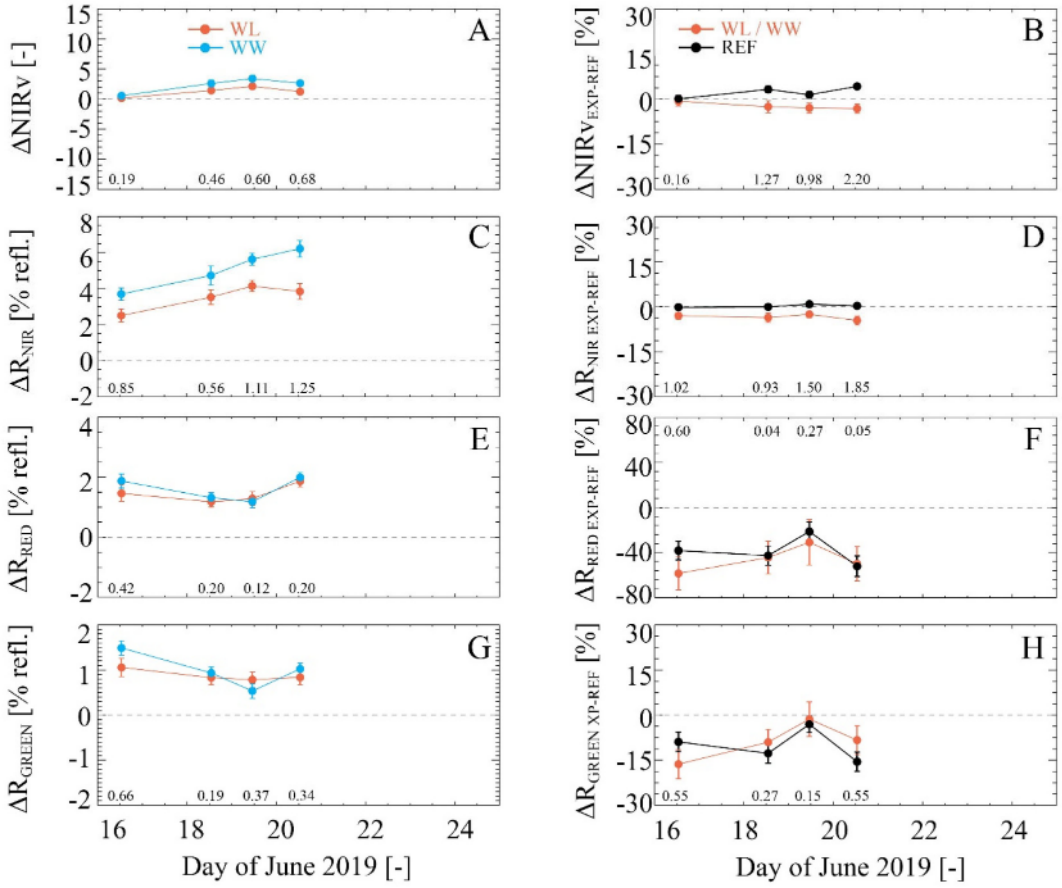

Fig. A5. Changes of remote sensing (RS) parameter during the water manipulation experiment in a maize canopy between 16 and 24 June 2019 acquired in the afternoon (13:30–14:30 CEST). Left column: Shown changes represented the difference of a certain RS parameter (P) compared to the first observation (16 June) in parameter units (ΔP) for the water-limited field (orange) and well-watered field (blue). Right column: percentage changes representing the relative difference between the water-limited and the well-watered area (orange), normalized considering the percentage change of the first day (16 June) ($\Delta P_{EXP\text{-}REF}$). The black line shows the normalized percent changes of two reference areas in the same plant rows not affected by the water-limitation experiment. Error bars indicate the 95% confidence interval and numbers the effect size (Cohen's d). (For interpretation of the references to colour in this figure legend, the reader is referred to the web version of this article.)

References

Badgley, G., Field, C.B., Berry, J.A., 2017. Canopy near-infrared reflectance and terrestrial photosynthesis. Sci. Adv. 3.

Barton, C.V.M., North, P.R.J., 2001. Remote sensing of canopy light use efficiency using the photochemical reflectance index - model and sensitivity analysis. Remote Sens. Environ. 78, 264–273.

Berk, A., Anderson, G.P., Acharya, P.K., Bernstein, L.S., Muratov, L., Lee, J., Fox, M., Adler-Golden, S.M., Chetwynd, J.H., Hoke, M.L., Lockwood, R.B., Gardner, J.A., Cooley, T.W., Borel, C.C., Lewis, P.E., 2005. MODTRAN5: A reformulated atmospheric band model with auxiliary species and practical multiple scattering options. Proc. Soc. Photo-Optical Instrument. Eng. 5655, 662–667.

Bonan, G.B., Williams, M., Fisher, R.A., Oleson, K.W., 2014. Modeling stomatal conductance in the earth system: linking leaf water-use efficiency and water transport along the soil–plant–atmosphere continuum. Geosci. Model Dev. 7, 2193–2222.

Cendrero-Mateo, M.P., Moran, M.S., Papuga, S.A., Thorp, K.R., Alonso, L., Moreno, J., Ponce-Campos, G., Rascher, U., Wang, G., 2016. Plant chlorophyll fluorescence: active and passive measurements at canopy and leaf scales with different nitrogen treatments. J. Exp. Bot. 67, 275–286.

Cendrero-Mateo, M.P., Wieneke, S., Damm, A., Alonso, L., Pinto, F., Moreno, J., Guanter, L., Celesti, M., Rossini, M., Sabater, N., Cogliati, S., Julitta, T., Rascher, U., Goulas, Y., Aasen, H., Pacheco-Labrador, J., Mac Arthur, A., 2019. Sun-induced chlorophyll fluorescence III: benchmarking retrieval methods and sensor characteristics for proximal sensing. Remote Sens. 11.

Ciais, P., Dolman, A.J., Bombelli, A., Duren, R., Peregon, A., Rayner, P.J., Miller, C., Gobron, N., Kinderman, G., Marland, G., Gruber, N., Chevallier, F., Andres, R.J., Balsamo, G., Bopp, L., Breon, F.M., Broquet, G., Dargaville, R., Battin, T.J., Borges, A., Bovensmann, H., Buchwitz, M., Butler, J., Canadell, J.G., Cook, R.B., DeFries, R., Engelen, R., Gurney, K.R., Heinze, C., Heimann, M., Held, A., Henry, M., Law, B., Luyssaert, S., Miller, J., Moriyama, T., Moulin, C., Myneni, R.B., Nussli, C., Obersteiner, M., Ojima, D., Pan, Y., Paris, J.D., Piao, S.L., Poulter, B., Plummer, S., Quegan, S., Raymond, P., Reichstein, M., Rivier, L., Sabine, C., Schimel, D., Tarasova, O., Valentini, R., Wang, R., van der Werf, G., Wickland, D., Williams, M., Zehner, C., 2014. Current systematic carbon-cycle observations and the need for implementing a policy-relevant carbon observing system. Biogeosciences 11, 3547–3602.

Cogliati, S., Celesti,, M., Cesana, I., Miglietta, F., Genesio, L., Julitta, T., Schuettemeyer, D., Drusch, M., Rascher, U., Jurado, P., Colombo, R., 2019. A spectral fitting algorithm to retrieve the fluorescence spectrum from canopy radiance. Remote Sens. 11 (16).

Cogliati, S., Verhoef, W., Kraft, S., Sabater, N., Alonso, L., Vicent, J., Moreno, J., Drusch, M., Colombo, R., 2015. Retrieval of sun-induced fluorescence using advanced spectral fitting methods. Remote Sens. Environ. 169, 344–357.

Damm, A., Erler, A., Hillen, W., Meroni, M., Schaepman, M.E., Verhoef, W., Rascher, U., 2011. Modeling the impact of spectral sensor configurations on the FLD retrieval accuracy of sun-induced chlorophyll fluorescence. Remote Sens. Environ. 115, 1882–1892.

Damm, A., Guanter, L., Verhoef, W., Schläpfer, D., Garbari, S., Schaepman, M.E., 2015. Impact of varying irradiance on vegetation indices and chlorophyll fluorescence derived from spectroscopy data. Remote Sens. Environ. 156, 202–215.

Damm, A., Paul-Limoges, E., Haghighi, E., Simmer, C., Morsdorf, F., Schneider, F.D., Van der Tol, C., Migliavacca, M., Rascher, U., 2018. Remote sensing of plant-water relations: an overview and future perspectives. J. Plant Physiol. 277, 3–19.

Dash, J., Curran, P.J., 2004. The MERIS terrestrial chlorophyll index. Int. J. Remote Sens. 25, 5403–5413.

Dolman, A.J., Miralles, D.G., de Jeu, R.A.M., 2014. Fifty years since Monteith's 1965 seminal paper: the emergence of global ecohydrology. Ecohydrology 7, 897–902.

Fawcett, D., Verhoef, W., Schläpfer, D., Schneider, F.D., Schaepman, M.E., Damm, A., 2018. Advancing retrievals of surface reflectance and vegetation indices over forest ecosystems by combining imaging spectroscopy, digital object models, and 3D canopy modelling. Remote Sens. Environ. 204, 583–595.

Feng, G., Yufang, J., Schaaf, C.B., Strahler, A.H., 2002. Bidirectional NDVI and atmospherically resistant BRDF inversion for vegetation canopy, - *40*, - 1278.
Gamon, J.A., Penuelas, J., Field, C.B., 1992. A narrow-waveband spectral index that tracks diurnal changes in photosynthetic efficiency. Remote Sens. Environ. 41, 35–44.
Garcia-Tejera, O., Lopez-Bernal, A., Testi, L., Villalobos, F.J., 2017. A soil-plant-atmosphere continuum (SPAC) model for simulating tree transpiration with a soil multi-compartment solution. Plant Soil 412, 215–233.
Gerhards, M., Rock, G., Schlerf, M., Udelhoven, T., 2016. Water stress detection in potato plants using leaf temperature, emissivity, and reflectance. Int. J. Appl. Earth Obs. Geoinf. 53, 27–39.
Guanter, L., Alonso, L., Gomez-Chova, L., Meroni, M., Preusker, R., Fischer, J., Moreno, J., 2010. Developments for vegetation fluorescence retrieval from spaceborne high-resolution spectrometry in the O2-A and O2-B absorption bands. J. Geophys. Res.-Atmos. 115.
Hanus, J., Fabianek, T., Fajmon, L., 2016. Potential of airborne imaging spectroscopy at czechglobe. In: Halounova, L., Safar, V., Toth, C.K., Karas, J., Huadong, G., Haala, N., Habib, A., Reinartz, P., Tang, X., Li, J., Armenakis, C., Grenzdorffer, G., LeRoux, P., Stylianidis, S., Blasi, R., Menard, M., Dufourmount, H., Li, Z. (Eds.), Xxiii Isprs Congress, Commission I, pp. 15–17.
Hueni, A., Damm, A., Kneubuehler, M., Schlapfer, D., Schaepman, M.E., 2017. Field and airborne spectroscopy cross validation-some considerations. IEEE J. Select. Top. Appl. Earth Observ. Remote Sens. 10, 1117–1135.
Jonard, F., de Canniere, S., Brüggemann, N., Gentine, P., Short Gianotti, D.J., Lobet, G., Miralles, D.G., Montzka, C., Pagán, B.R., Rascher, U., Vereecken, H., 2020. Value of sun-induced chlorophyll fluorescence for quantifying hydrologicalstates and fluxes: current status and challenges. Agric. For. Meteorol. 291.
Kückenbrink, D., Hueni, A., Damm, A., Schneider, F.D., Gastellu-Etchegorry, J.P., Schaepman, M.E., Morsdorf, F., 2019. Mapping the irradiance field of a single tree: quantifying vegetation induced adjacency effects. IEEE Trans. Geosci. Remote Sensing 57 (7), 4994–5011. *8645789*.
Li, X., Gentine, P., Lin, C., Zhou, S., Sun, Z., Zheng, Y., Liu, J., Zheng, C., 2019. A simple and objective method to partition evapotranspiration into transpiration and evaporation at eddy-covariance sites. Agric. For. Meteorol. 265, 171–182.
Meroni, M., Busetto, L., Colombo, R., Guanter, L., Moreno, J., Verhoef, W., 2010. Performance of spectral fitting methods for vegetation fluorescence quantification. Remote Sens. Environ. 114, 363–374.
Miralles, D.G., Gentine, P., Seneviratne, S.I., Teuling, A.J., 2019. Land-atmospheric feedbacks during droughts and heatwaves: state of the science and current challenges. Ann. N. Y. Acad. Sci. 1436, 19–35.
Mohammed, G., Colombo, R., Middleton, E., Rascher, U., van der Tol, C., Berry, J.A.L.N., Goulas, Y., Perez-Priego, O., Damm, A., Meroni, M., Joiner, J., Cogliati, S., Verhoef, W., Gastellu-Etchegorry, J.P., Malenovský, Z., Miller, J.R., Guanter, L., Moreno, J., Moya, I., Frankenberg, C., Zarco-Tejada, P.J., 2019. Remote sensing of solar-induced chlorophyll fluorescence (SIF) in vegetation: 50 years of progress. Remote Sens. Environ. 231, 111177.
Myneni, R.B., Maggion, S., Iaquinto, J., Privette, J.L., Gobron, N., Pinty, B., Kimes, D.S., Verstraete, M.M., Williams, D.L., 1995. Optical remote-sensing of vegetation - modeling, caveats, and algorithms. Remote Sens. Environ. 51, 169–188.
Penuelas, J., Filella, I., Biel, C., Serrano, L., Save, R., 1993. The reflectance at the 950-970 nm region as an indicator of plant water status. Int. J. Remote Sens. 14, 1887–1905.
Peressotti, A., Ham, J.M., 1996. A dual-heater gauge for measuring sap flow with an improved heat-balance method. Agron. J. 88, 149–155.
Porcar-Castell, A., Malenovský, Z., Magney, T., Van Wittenberghe, S., Fernández-Marín, B., Maignan, F., Zhang, Y., Maseyk, K., Atherton, J., Albert, L.P., Robson, T. M., Zhao, F., Garcia-Plazaola, J.-I., Ensminger, I., Rajewicz, P.A., Grebe, S., Tikkanen, M., Kellner, J.R., Ihalainen, J.A., Rascher, U., Logan, B., 2021. Chlorophyll a fluorescence illuminates a path connecting plant molecular biology to earth-system science. Nature Plants 7, 998–1009.
Rascher, U., Alonso, L., Burkhart, A., Cilia, C., Cogliati, S., Colombo, R., Damm, A., Drusch, M., Guanter, L., Hanus, J., Hyvärinen, T., Julitta, T., Jussila, J., Katajak, K., Kokkalis, P., Kraft, S., Kraska, T., Matveeva, M., Moreno, J., Muller, O., Panigada, C., Pikl, M., Pinto, F., Prey, L., Pude, R., Rossini, M., Schickling, A., Schurr, U., Schüttemeyer, D., Verrelst, J., Zemek, F., 2015. Sun-induced fluorescence - a new probe of photosynthesis: first maps from the imaging spectrometer HyPlant. Glob. Chang. Biol. 21, 4673–4684.
Reichstein, M., Bahn, M., Ciais, P., Frank, D., Mahecha, M.D., Seneviratne, S.I., Zscheischler, J., Beer, C., Buchmann, N., Frank, D.C., Papale, D., Rammig, A., Smith, P., Thonicke, K., Van Der Velde, M., Vicca, S., Walz, A., Wattenbach, M., 2013. Climate extremes and the carbon cycle. Nature 500, 287–295.
Ryu, Y., Berry, J.A., Baldocchi, D.D., 2019. What is global photosynthesis? History, uncertainties and opportunities. Remote Sens. Environ. 223, 95–114.
Sakuratani, T., 1981. A heat balance method for measuring water flux in the stem of intact plants. J. Agric. Meteorol. 37.
Scholander, P.F., Hammel, H.T., Bradstreet, E.D., Hemmingsen, E.A., 1965. Sap pressure in vascular plants - negative hydrostatic pressure can be measured in plants. Science 148, 339-+.
Schuldt, B., Buras, A., Ahrend, M., Vitasse, Y., Beierkuhnlein, C., Damm, A., Gharun, M., Grams, T., Hauck, M., Hajek, P., Hartmann, H., Hilbrunner, E., Hoch, G., Holloway-Phillips, M., Körner, C., Larysch, E., Lübbe, T., Nelson, D.B., Rammig, A., Rigling, A., Rose, L., Ruehr, N.K., Schumann, K., Weiser, K., Werner, C., Wohlgemuth, T., Zang, C., Kahmen, A., 2020. A first assessment of the impact of the extreme 2018 summer drought on Central European forests. Basic Appl. Ecol. 45, 86–103.
Shan, N., Ju, W., Migliavacca, M., Martini, D., Guanter, L., Chen, J., Goulas, Y., Zhang, Y., 2019. Modeling canopy conductance and transpiration from solar-induced chlorophyll fluorescence. Agric. For. Meteorol. 268, 189–201.
Siegmann, B., Alonso, L., Celesti, M., Cogliati, S., Colombo, R., Damm, A., Douglas, S., Guanter, L., Hanuš, J., Kataja, K., Kraska, T., Matveeva, M., Moreno, J., Muller, O., Pikl, M., Pinto, F., Vargas, J.Q., Rademske, P., Rodriguez-Morene, F., Sabater, N., Schickling, A., Schüttemeyer, D., Zemek, F., Rascher, U., 2019. The high-performance airborne imaging spectrometer HyPlant-from raw images to top-of-canopy reflectance and fluorescence products: introduction of an automatized processing chain. Remote Sens. 11.
Sippel, S., Reichstein, M., Ma, X.L., Mahecha, M.D., Lange, H., Flach, M., Frank, D., 2018. Drought, heat, and the carbon cycle. Curr. Climate Change Rep. 4, 266–286.
Sippel, S., Meinshausen, N., Fischer, E.M., Szekely, E., Knutti, R., 2020. Climate change now detectable from any single day of weather at global scale. Nat. Clim. Chang. 10, 35-+.
Smith, M.D., 2011. An ecological perspective on extreme climatic events: a synthetic definition and framework to guide future research. J. Ecol. 99, 656–663.
Stocker, B.D., Zscheischler, J., Keenan, T.F., Prentice, I.C., Seneviratne, S.I., Peñuelas, J., 2019. Drought impacts on terrestrial primary production underestimated by satellite monitoring. Nat. Geosci. 12, 264–270.
Sun, Y., Fu, R., Dickinson, R., Joiner, J., Frankenberg, C., Gu, L.H., Xia, Y.L., Fernando, N., 2015. Drought onset mechanisms revealed by satellite solar-induced chlorophyll fluorescence: insights from two contrasting extreme events. J. Geophys. Res.-Biogeosci. 120, 2427–2440.
Talsma, C.J., Good, S.P., Jimenez, C., Martens, B., Fisher, J.B., Miralles, D.G., McCabe, M. F., Purdy, A.J., 2018. Partitioning of evapotranspiration in remote sensing-based models. Agric. For. Meteorol. 260-261, 131–143.
Turner, N.C., Long, M.J., 1980. Errors arising from rapid water-loss in the measurement of LEAF water potential by the pressure chamber technique. Aust. J. Plant Physiol. 7, 527–537.
van der Tol, C., Verhoef, W., Rosema, A., 2009. A model for chlorophyll fluorescence and photosynthesis at leaf scale. Agric. For. Meteorol. 149, 96–105.
Van Wittenberghe, S., Laparra, V., Ignacio Garcia-Plazaola, J., Fernandez-Marin, B., Porcar-Castell, A., Moreno, J., 2021. Combined dynamics of the 500–600 nm leaf absorption and chlorophyll fluorescence changes in vivo: Evidence for the multifunctional energy quenching role of xanthophylls. BBA-Bioenergetics 1862.
Verhoef, W., van der Tol, C., Middleton M., E., 2018. Hyperspectral radiative transfer modeling to explore the combined retrieval of biophysical parameters and canopy fluorescence from FLEX - Sentinel-3 tandem mission multi-sensor data. Remote Sens. Environ. 204, 942–963.
von Buttlar, J., Zscheischler, J., Rammig, A., Sippel, S., Reichstein, M., Knohl, A., Jung, M., Menzer, O., Arain, M.A., Buchmann, N., Cescatti, A., Gianelle, D., Kiely, G., Law, B.E., Magliulo, V., Margolis, H., McCaughey, H., Merbold, L., Migliavacca, M., Montagnani, L., Oechel, W., Pavelka, M., Peichl, M., Rambal, S., Raschi, A., Scott, R. L., Vaccari, F.P., van Gorsel, E., Varlagin, A., Wohlfahrt, G., Mahecha, M.D., 2018. Impacts of droughts and extreme-temperature events on gross primary production and ecosystem respiration: a systematic assessment across ecosystems and climate zones. Biogeosciences 15, 1293–1318.
Wang, K.C., Dickinson, R.E., 2012. A review of gobal terrestrial evapotranspiration: observation, modeling, climatology, and climatic variability. Rev. Geophys. 50.
Weyermann, J., Damm, A., Kneubuehler, M., Schaepman, M.E., 2014. Correction of reflectance anisotropy effects of vegetation on airborne spectroscopy data and derived products. IEEE Trans. Geosci. Remote Sens. 52, 616–627.
Yang, P., van der Tol, C., Verhoef, W., Damm, A., Schickling, A., Kraska, T., Muller, O., Rascher, U., 2019. Using reflectance to explain vegetation biochemical and structural effects on sun-induced chlorophyll fluorescence. Remote Sens. Environ. 231, 110996.
Yoshida, Y., Joiner, J., Tucker, C., Berry, J., Lee, J.E., Walker, G., Reichle, R., Koster, R., Lyapustin, A., Wang, Y., 2015. The 2010 Russian drought impact on satellite measurements of solar-induced chlorophyll fluorescence: insights from modeling and comparisons with parameters derived from satellite reflectances. Remote Sens. Environ. 166, 163–177.
Zarco-Tejada, P.J., Gonzalez-Dugo, V., Berni, J.A.J., 2012. Fluorescence, temperature and narrow-band indices acquired from a UAV platform for water stress detection using a micro-hyperspectral imager and a thermal camera. Remote Sens. Environ. 117, 322–337.
Zeng, Y., Chen, M., Hao, D., Damm, A., Badgley, G., Rascher, U., Johnson, J.E., Dechant, B., Siegmann, B., Ryu, Y., Qiu, H., Krieger, V., Panigada, C., Celesti, M., Miglietta, F., Yang, X., Berry, J.A., 2022. Combining near-infrared radiance of vegetation and fluorescence spectroscopy to detect effects of abiotic changes and stresses. Remote Sens. Environ. 270, 112856.